Size and shape dependent photoluminescence and excited state decay rates of diamondoids

Robert Richter,*[a] David Wolter,[a] Tobias Zimmermann,[a] Lasse Landt,[a] Andre Knecht,[a] Christoph Heidrich,[a] Andrea Merli,[a] Otto Dopfer,[a] Philipp Reiß,[b] Arno Ehresmann,[b] Jens Petersen,[c] Jeremy E. Dahl,[d] Robert M. K. Carlson,[d] Christoph Bostedt,[e] Thomas Möller,[a] Roland Mitric[c] and Torbjörn Rander*[a]

We present photoluminescence spectra and excited state decay rates of a series of diamondoids, which represent molecular structural analogues to hydrogen-passivated bulk diamond. Specific isomers of the five smallest diamondoids (adamantane–pentamantane) have been brought into the gas phase and irradiated with synchrotron radiation. All investigated compounds show intrinsic photoluminescence in the ultraviolet spectral region. The emission spectra exhibit pronounced vibrational fine structure which is analyzed using quantum chemical calculations. We show that the geometrical relaxation of the first excited state of adamantane, exhibiting Rydberg character, leads to the loss of T_d symmetry. The luminescence of adamantane is attributed to a transition from the delocalized first excited state into different vibrational modes of the electronic ground state. Similar geometrical changes of the excited state structure have also been identified in the other investigated diamondoids. The excited state decay rates show a clear dependence on the size of the diamondoid, but are independent of the particle geometry, further indicating a loss of particle symmetry upon electronic excitation.

1 Introduction

The size- and shape-dependent optical properties of nanocrystals have attracted great interest in recent years.[1–4] Such systems are promising candidates for tuning of optical properties,[5–7] with a variety of applications ranging from molecular building blocks for optoelectronics to biocompatible, photostable biomarkers.[8–15] In particular, the observation of photoluminescence (PL) in reduced-dimensional semiconductor systems, which otherwise exhibit an indirect band gap, like Si and C (diamond), opens possibilities to tailor their optical properties and to interface with already existing technologies.[2–4] However, despite numerous studies,[2–4,16,17] the fundamental photophysical processes in such systems still are not fully understood. In order to gain a deeper insight into these processes, it is desirable to perform experiments under idealized conditions, *i.e.* on electrically neutral, isolated systems with well defined sizes and structures. Such an approach enables the direct comparison with theoretical calculations.

Diamondoids can be considered structurally as fragments of the diamond lattice (Fig. 1). At the same time, they belong to the hydrocarbon class of molecules, where the free valences of the carbon atoms are saturated by hydrogen. This is similar to the surface passivation by hydrogen present in macroscopic diamond produced by chemical vapor deposition (CVD).[18,19] All carbon atoms in pristine diamondoids are sp^3-hybridized, resulting in three-dimensional cage-like structures. Corresponding to the number of cages, a numerical multiplier (dia-, tria-, tetra-, and pentamantane) is used for naming the polymantanes. Ada-, dia-, and triamantane are called lower diamondoids, and each has only one structural isomer congruent with the diamond lattice. For the higher diamondoids, the number of isomers increases drastically with the number of cages. Chirality aside, tetramantane has three isomers, pentamantane six, and hexamantane already 24. The notation for different isomers usually follows the nomenclature of Balaban and Schleyer (see Table 1).[20] Diamondoids are perfectly size- and shape-selectable, which makes them ideal model systems for the study of how size and shape affect the properties of nanoparticles.[21,22]

The PL of gas phase adamantane has been previously studied.[2] However, the experimental parameters (*i.e.* high excitation energies with respect to the optical gap [E_{gap}]) caused the spectrum to be

[a] Institut für Optik und Atomare Physik, Technische Universität Berlin, Hardenbergstr. 36, 10623 Berlin, Germany. E-mail: robert.richter@tu-berlin.de

[b] Institute of Physics and Center for Interdisciplinary Nanostructure Science and Technology (CINSaT), University of Kassel, Heinrich-Plett-Str. 40, 34132 Kassel, Germany

[c] Universität Würzburg, Institut für Physikalische und Theoretische Chemie, Am Hubland, 97074 Würzburg, Germany

[d] Stanford Institute for Materials and Energy Sciences, Stanford University, Stanford, California 94305, USA

[e] SLAC National Accelerator Laboratory, Menlo Park, California 94025, USA

3070 | *Phys. Chem. Chem. Phys.*, 2014, **16**, 3070–3076

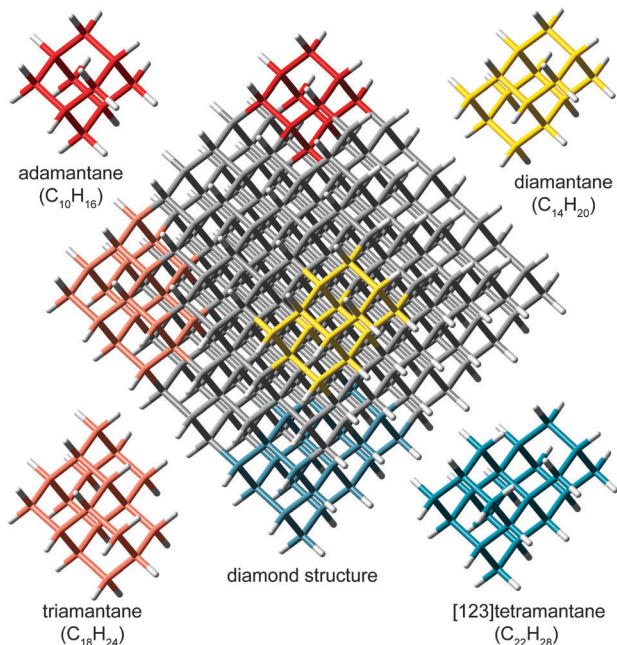This journal is © the Owner Societies 2014

Fig. 1   Examples of diamondoids, surface hydrogen atoms are shown in white.

Table 1   Estimated sublimation temperatures T_s, optical gaps E_{gap}, excited state decay rates $1/\tau$, ground state symmetries, molecular formulae of the investigated compounds, and excitation energies used in the PL measurements

n-Mantane	T_s (°C)	$E_{gap}{}^b$ (eV)	$1/\tau$ (ns^{-1})	Symmetry	Formula	Excitation energy (eV)
Ada	25	6.49	0.75 ± 0.02	T_d	$C_{10}H_{16}$	6.49
Dia	60	6.40	1.39 ± 0.06	D_{3d}	$C_{14}H_{20}$	6.60
Tria	90	6.06	1.72 ± 0.09	C_{2v}	$C_{18}H_{24}$	6.78
[121]Tetra	140	6.10	—	C_{2h}	$C_{22}H_{28}$	6.88
[1(2)3]Tetra	140	5.94	2.13 ± 0.15	C_{3v}	$C_{22}H_{28}$	5.99
[123]Tetra^a	140	5.95	2.32 ± 0.17	C_2	$C_{22}H_{28}$	5.98
[1(2,3)4]Penta	160	5.81	3.13 ± 0.32	T_d	$C_{26}H_{32}$	5.93
[12(1)3]Penta^a	160	5.83	2.38 ± 0.18	C_1	$C_{26}H_{32}$	6.20
[1212]Penta	160	5.85	—	C_{2v}	$C_{26}H_{32}$	—
[1213]Penta^a	160	5.79	2.77 ± 0.25	C_1	$C_{26}H_{32}$	6.31
[12(3)4]Penta	160	—	—	C_s	$C_{26}H_{32}$	—
[1234]Penta^a	160	—	—	C_2	$C_{26}H_{32}$	—
[12312]Hexa	160	5.88	—	D_{3d}	$C_{26}H_{30}$	—

^{a} Samples are racemic mixtures.[22] ^{b} Gaps from ref. 1 and 32.

completely congested, thus lacking any vibrational fine structure, making it difficult to compare with calculations.[16] The optical properties of gas phase polymantanes have so far only been investigated with absorption spectroscopy.[2] This study showed that the basic shape (1-, 2-, & 3-dimensional) of the diamondoids is reflected in the overall shape of its absorption spectrum. In addition, the recent theoretical work of Patrick and Giustino[23] has shown that including the nuclear dynamics in the analysis is key to understanding the complicated absorption spectra. It has also been shown that functionalization with a thiol group lowers the optical gap and quenches PL.[1] The PL of higher diamondoids has, so far, been examined only in diamondoid crystals, where it is a property of the molecular solid.[17] In this work, we present the first PL spectra of higher diamondoids in the gas phase, and their excited state decay rates.

2 Experimental section

Although considerable progress has been made in recent years, synthesis of higher diamondoids still presents a major challenge.[22,24–27] All samples used in this work, except adamantane, were extracted from crude oil and subsequently purified *via* vacuum distillation and pyrolysis. Size and shape selection was achieved by high-performance liquid chromatography. Further details of the extraction and characterization can be found in the work of Dahl *et al.*[22] Adamantane was purchased from Sigma Aldrich. All samples had a purity of >99%. To ensure that the observed fluorescence stemmed from the diamondoids, fluorescence excitation spectra were recorded which reflect their absorption spectra (not shown). For the PL measurements the samples were brought into the gas phase using a heatable target cell with UV-transparent MgF$_2$-windows. The cell, including the samples, was outgassed at elevated temperatures until the ambient pressure was less than 10^{-5} mbar. Prior to reaching the sublimation temperature T_s of each sample, the target cell was sealed. To minimize thermal broadening of the spectra, the temperature of the target cell during the measurement was kept only slightly above T_s (see Table 1). In order to introduce as little excess energy as possible into the system, *i.e.* to reduce broadening from intramolecular vibrational energy redistribution (IVR),[28] the excitation energies were chosen close to E_{gap}. However, in some cases the choice of excitation energy was limited by a low absorption cross section.

The experiments were performed at the U125/2 10m-NIM[29] beamline at the BESSY II synchrotron radiation facility (Helmholtz-Zentrum Berlin, Germany). The PL spectra were recorded using either a Seya-Namioka or a Czerny–Turner type spectrometer with a position sensitive detector equipped with a CsTe coated microchannel plate or a cooled CCD detector, respectively. The spectral resolution ΔE for each spectrum is given in the figure captions. Excited state decay rates were measured using time-correlated single photon counting. As a periodical excitation light source, we employed the light produced by the 10 mA single bunch of the Multi Bunch Hybrid Mode at BESSY II. Luminescence photons were counted using a Hamamatsu R7400P-06 fast photomultiplier tube, sensitive between 1.9 and 7.75 eV. A SiO$_2$-lens was used to focus the luminescence light onto the photomultiplier tube and as a long-pass edge filter with a cut-off energy of about 6.6 eV. By choosing excitation energies of above 6.6 eV, detection of scattered photons from the incident light beam could be avoided. The fluorescence decay signal was deconvolved from the instrument function by a least-square procedure.[30,31]

3 Computational methods

The vibrationally resolved optical absorption and emission spectra of adamantane were calculated based on the Franck–Condon principle[33,34] using the method of Santoro *et al.*[35,36] as implemented in the Gaussian 09 quantum chemical software package.[37] This approach involves the calculation of vibrational normal modes for the optimized geometries of the ground and excited electronic states contributing to the studied vibronic band, followed by the computation of Franck–Condon factors for the individual

combinations of vibrational states. For this purpose, the Duschinsky transformation between the normal modes of the ground and excited electronic state is performed,[38] and the Franck–Condon factors are obtained analytically utilizing a recursive procedure.[39] In the present calculations, only transitions from the vibrational ground state of the initial electronic state to the manifold of vibrational states of the final electronic state were taken into account. The electronic structure was described using density functional theory (DFT) for the electronic ground state and time-dependent density functional theory (TDDFT) for the excited states. Due to the Rydberg character of the low-lying electronically excited states of adamantane, the long-range-corrected CAM-B3LYP functional[40] combined with the 6-311++G** basis set[41] containing diffuse basis functions was employed. This ensures an accurate description of these states, as is evident from the very good agreement between the theoretical and experimental spectra. The calculated stick absorption and emission spectra were convolved with a Gaussian function in order to obtain better comparability with the experimental data. For the absorption spectra, a full width at half maximum (FWHM) of 10 meV was employed, while for emission the FWHM was 20 meV.

4 Results and discussion

In the following, we first discuss the luminescence spectrum of adamantane and analyze it by comparison to the theoretical calculations. Subsequently, the experimental photoluminescence of the polymantanes is presented and compared to that of adamantane. Finally, the excited state decay rates are discussed.

4.1 Photoluminescence of adamantane

The experimental and theoretical photoluminescence and absorption spectra of adamantane are presented in Fig. 2. Partly resolved vibrational fine structure is apparent in the measured spectra and reproduced with good agreement by the calculations.

Landt et al.[2] previously published a similar PL-spectrum, but obtained using a higher excitation energy. They observed a broad, structureless PL which was explained through a self-trapped exciton. Our new data suggest that the previous observation results from broadening due to thermal effects and IVR, where the excess energy provided by the photon is dissipated among the vibrational degrees of freedom.

The experimental data as well as the calculations show that the energetically highest emission feature coincides with the first allowed transition in absorption. This result suggests that for the PL of adamantane the initial state is the vibrational ground state of the first optically allowed excited singlet state (S_1) which exhibits 3s-like Rydberg character.[43,44] The vibrational progressions in the PL spectrum are determined mainly by five normal modes of the electronic ground state S_0. The modes with the largest contribution are labelled in Table 2. The calculated energies, assignments and symmetries are listed in Table 3. A large number of combinations of these normal modes contribute to the broad background. The maximum
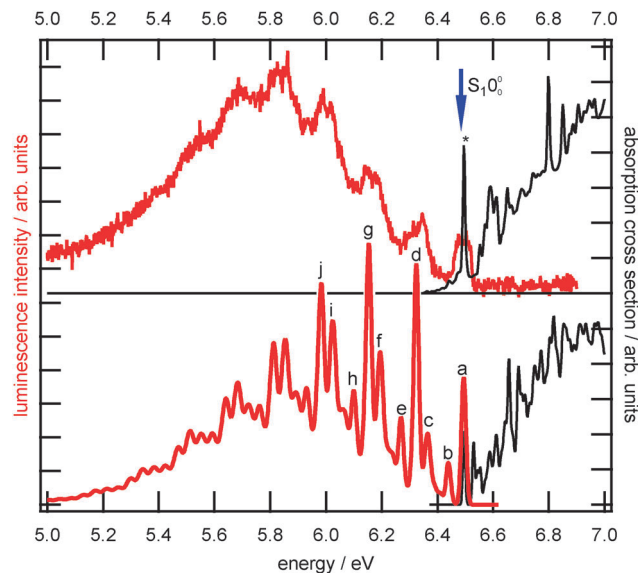

Fig. 2 Measured (top) and calculated (bottom) PL (red) and absorption (black) spectra of adamantane. The excitation energy is marked with an asterisk and E_{gap} is marked with a blue arrow. The experimental resolution ΔE of the absorption is 10 meV, while the resolution in the PL is 100 meV. The calculated PL and absorption spectra were convolved with a Gaussian function with a FWHM of 20 and 10 meV and redshifted by 60 meV.

Table 2 Assignment of the vibrational normal modes that are the main contributors to the peaks in the calculated PL spectrum of adamantane. The modes are denoted by ν_b, where ν is the mode and b the number of quanta in this mode. The modes were numbered according to increasing energy. Different contributions are separated by commas. Simultaneous excitation of different modes is indicated by slash

Peak	Main contribution
a	0–0
b	6_1
c	21_1, 24_1
d	40_1, 41_1
e	$41_1/6_1$
f	$41_1/21_1$, $41_1/24_1$
g	41_2, 40_2, $40_1/41_1$
h	$41_2/6_1$
i	$41_2/24_1$
j	$40_1/41_2$, $40_2/41_1$

Table 3 Calculated energies, assignments and symmetries of vibrational normal modes that are the main contributors to the peaks in the calculated PL-spectrum of adamantane. Assignments and symmetries from Jensen et al.[42]

Mode	Energy (cm^{-1}/meV)	Assignment	Symmetry
6	459/57	C–C–C wag	t_1
21	993/123	C–C stretch	t_2
24	1069/133	C–C–C bend	a_1
40	1364/169	C–H wag	t_2
41	1364/169	C–H wag	t_2

intensity of the emission is red-shifted by roughly 0.8 eV with respect to the adiabatic 0–0 transition between the lowest vibrational levels of both electronic states ($S_10_0^0$, see Fig. 2).
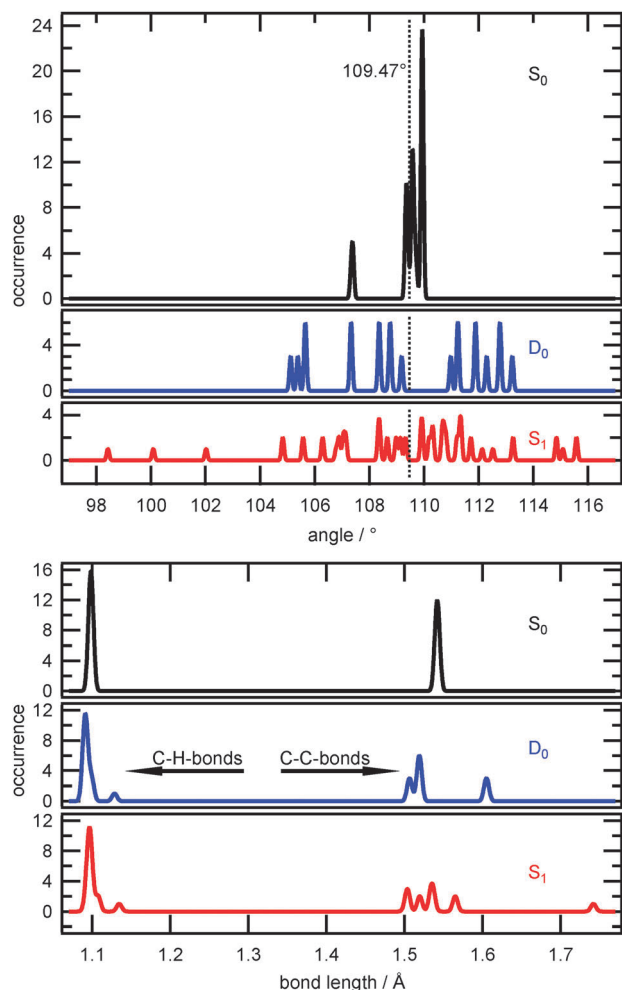
3072 | *Phys. Chem. Chem. Phys.*, 2014, **16**, 3070–3076

This journal is © the Owner Societies 2014

Fig. 3   Calculated angular distributions (top) and bond lengths (bottom) of the ground state S_0 (black), the relaxed excited state S_1 (red) and the cation D_0 (blue) of adamantane.

This observation indicates a substantial change in the geometry upon electronic excitation, which is supported by the calculated relaxed structures of the ground and the excited states. A previous study has shown that the adamantane cation is significantly Jahn–Teller-distorted.[8] We compare our computed values of the ground and first excited states of adamantane to the adamantane cation ground state D_0 in Fig. 3.

The discrete values have been convolved with a Gaussian function to account for small deviations due to the numerical error inherent in the DFT procedure. In an idealized structure of adamantane, the angle spanned by any three neighboring atoms is the tetrahedral edge central angle with a value of $\sim 109.47°$. The T_d-symmetry can be conserved when some angles differ. However, certain sets of angles have to do so collectively (for example: all H–C–H angles have to be the same for the structure to maintain T_d-symmetry). While the bond lengths and angles of the electronic ground state are confined to a few values, the results for the relaxed excited state and the cation show strong deviations in the bond length and angular distributions. Compared to the ground state values, bond lengths vary up to

8% for the excited state and 4% for the cation while the angles differ by up to $14°$ for the excited state and up to $5°$ for the cation. This indicates a lowering of the molecular symmetry in the excited state. To quantitatively investigate this effect we calculated the root mean square deviation (RMSD) from the idealized structure with perfect T_d-symmetry.[45] The RMSD of the optimized ground state structure of adamantane amounts to 1.9×10^{-3} Å, which is roughly one order of magnitude smaller than the RMSD of both the excited state structure with 4.7×10^{-2} Å and of the cation with 4.0×10^{-2} Å. For the cation, it has been found previously that the symmetry is lowered to C_{3v}.[8]

It is worth noting that the angles of the cation appear in 13 sets (see Fig. 3). Of these sets, 7 have an occurrence of 6, while the 6 remaining sets each have a value that occurs 3 times, adding up to the 60 angles in adamantane. Although calculated *without* symmetry restrictions, the C_{3v} symmetry of the cation is reflected in the degeneracy of these values. The angular distribution of the S_1 state structure, in contrast, contains several angles of which the values occur only once, with large deviations to other angles. Thus, in the framework of the TDDFT approach employed, the S_1 state seems to exhibit an even lower symmetry than the D_0 state in the cation. The relaxed S_0 and S_1 state geometries can be seen in Fig. 4, where
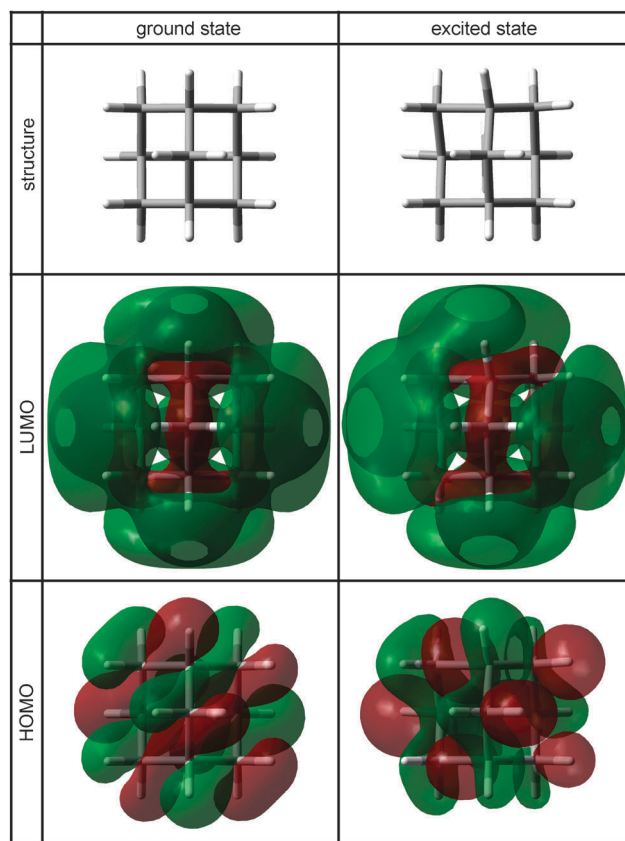

Fig. 4   Calculated geometrical structure and iso-surfaces of the LUMO and the HOMO for the ground and the excited state of adamantane. The orbitals are shown with an isovalue of 0.018.

This journal is © the Owner Societies 2014

Phys. Chem. Chem. Phys., 2014, **16**, 3070–3076 | **3073**

their highest occupied molecular orbitals (HOMO) and lowest unoccupied molecular orbitals (LUMO) are shown. The excitation between these orbitals provides the main contribution to the S_0–S_1 transition in adamantane. While the LUMO and HOMO of the ground state structure are highly symmetric, both molecular orbitals are considerably distorted in the relaxed excited state. This shows that even though the Rydberg state is characterized by a relatively diffuse electron distribution, the transition to this state affects the nuclear configuration of the molecule, as can be seen in Fig. 3 and 4.

4.2 Photoluminescence of the polymantanes

Fig. 5 shows the PL as well as the absorption spectra of all investigated polymantanes. The absorption spectra (black) and E_{gap} (blue arrow) have been taken from Landt et al.[1] The excitation energy used to record the individual PL spectra (red) is marked with an asterisk. Similar to the case of adamantane, the PL spectra of the polymantanes are dominated by vibronic progressions that get congested by thermal inhomogeneous broadening (TIB), and IVR in cases where the excitation energy is much higher than E_{gap}. Since the highest energy of emission in all the polymantanes is very close to E_{gap} of the respective sample, it is reasonable to assume that in all cases, the S_1 state is the preferred initial state for the luminescence. The vertical energy shift of the vibrational envelope in emission with respect to E_{gap} indicates that also polymantanes undergo a significant change in geometry upon excitation.

Each diamondoid has a unique luminescence spectrum, most with pronounced vibrational progressions. The varying appearances of the spectra can be readily explained with the unique symmetry selection rules for the vibrational normal modes of the individual isomers. Ground state symmetries are listed in Table 1. Landt et al. have pointed out that for some species (diamantane and [121]tetramantane in our sample series), a smooth absorption onset is observed. It was shown by Vörös et al. that in these cases, the lowest transition is dipole forbidden[43] in the initial D_{3d} and C_{2h} symmetries.

Hence, E_{gap} is no longer related to the transition to the first excited state of the polymantane, which is dominated by the HOMO to LUMO orbital excitation and has 3s Rydberg character. Rather, a higher-lying excited electronic state is populated which may be dominated by HOMO to LUMO + 1 or HOMO to LUMO + 2 orbital excitations exhibiting 3p Rydberg character.[43] However, nonetheless, the PL in these systems presumably occurs from the first excited state, which may be reached by non-radiative internal conversion processes from the initially populated states. This can be accompanied by a lowering of the molecular symmetry and hence increased transition moments to the ground state. The detailed theoretical simulation of the dynamical electronic and vibrational relaxation processes in diamondoids is currently in progress.[46] The initial excitation to higher-lying states together with the non-radiative relaxation processes that result in the transformation of electronic into vibrational energy lead to thermal broadening and stronger IVR, both causing the spectra to exhibit less fine-structure than those of the other diamondoids.
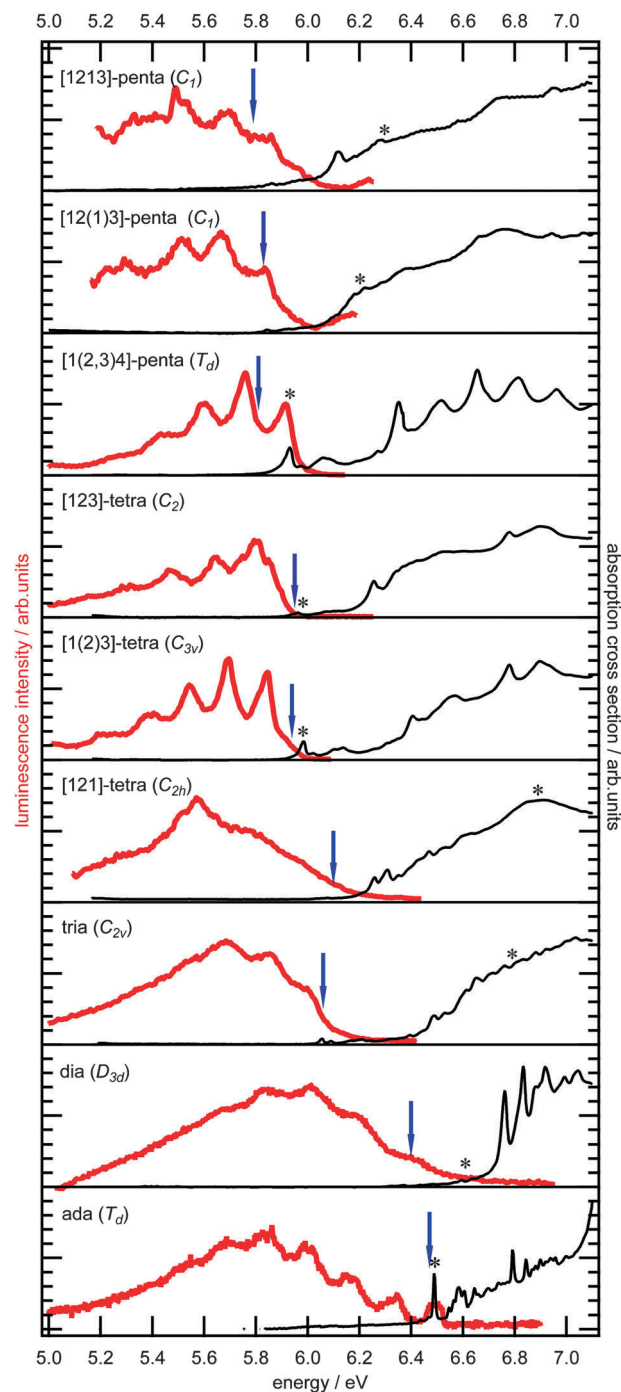

Fig. 5   Measured photoluminescence spectra (red) and absorption spectra (black) of selected isomers of the five smallest members of the diamondoid series. The excitation energy used to record the PL is marked with an asterisk and E_{gap} is marked with a blue arrow. PL-spectra of adamantane ($\Delta E = 100$ meV), diamantane ($\Delta E = 100$ meV), other spectra ($\Delta E = 25$ meV, the spectra have been smoothed for presentation purposes).

4.3 Excited-state decay rates

The measured decay rates of all investigated diamondoids are listed in Table 1. To rule out that the temperature of the samples affect their excited state decay rates ($1/\tau$) we recorded them at different temperatures for ada- and diamantane.
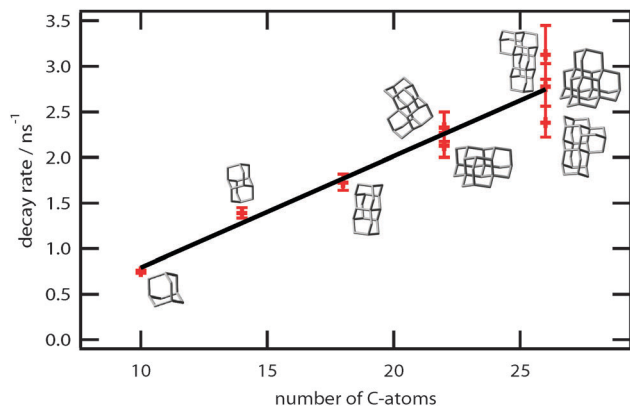
Fig. 6 Excited state decay rates of the diamondoids as a function of the number of constituent C-atoms.

Within our experimental error, temperature does not have an influence on the decay rate of the excited state.

As can be seen from Fig. 6, the decay rates are not related in a simple way to the particle symmetry. This is most likely due to the fact that for larger particles, the number of degrees of freedom over which IVR can take place is a more important quantity in determining the decay rates. In Fig. 6, the decay rate as a function of the number of C-atoms of the diamondoid is shown. The decay rate is seen to increase monotonically with increasing diamondoid order, and in a simple picture, the correlation between size and the transition rate can be approximated by a linear dependence of 0.12 ns^{-1} per additional carbon atom. This dependence may result from the fact that internal conversion mechanisms like IVR are strongly dependent on the number of available vibrational degrees of freedom. These processes are known to take place on time scales much shorter than the observed lifetimes, and PL mainly takes place after the internal conversion is complete. Hence, it is conceivable that systems with a higher number of atoms also have higher decay rates. However, with these initial results, it is not possible to determine the branching ratio between radiative and non-radiative processes.

5 Conclusion

We have shown that all diamondoids up to a size of ∼1 nm exhibit PL in the ultraviolet spectral region. Under carefully controlled experimental conditions (low temperature and low excitation energy) vibrational fine structure could be observed. The broad and structureless PL spectra published in previous work were presumably the result of thermal broadening and broadening due to IVR. The luminescence of adamantane, including its vibrational fine structure, can be explained by a transition from a delocalized 3s-like Rydberg state into mainly five vibrational normal modes of the ground state. Furthermore, the PL properties of the five smallest diamondoids can also be explained through the same scheme, except for cases where the HOMO–LUMO transition is dipole forbidden (diamantane, [121]tetramantane), where the initial excitation occurs to a

higher-lying 3p Rydberg state. In the latter cases, fluorescence is emitted from a lower lying state and the PL spectra are smeared out due to an increased amount of IVR.

The unique spectral shape observed not only for each size, but also for each isomer of the diamondoid series, shows that our technique can be used to optically probe sizes and structural traits. This could be helpful for monitoring the synthesis of higher diamondoids and is a step towards a better general understanding of the PL properties of semi-conductor nanoparticles. The ability of theory to model the PL spectra proved to be vital to the assignment of the vibrational spectra, and the synergies between further developing the theoretical description of these processes and improved experiments provide a very strong impetus for new developments in the field.

Acknowledgements

References

1 L. Landt, K. Klünder, J. E. Dahl, R. M. K. Carlson, T. Möller and C. Bostedt, *Phys. Rev. Lett.*, 2009, **103**, 1–4.
2 L. Landt, W. Kielich, D. Wolter, M. Staiger, A. Ehresmann, T. Möller and C. Bostedt, *Phys. Rev. B: Condens. Matter Mater. Phys.*, 2009, **80**, 10–13.
3 T. van Buuren, L. Dinh, L. Chase, W. Siekhaus and L. Terminello, *Phys. Rev. Lett.*, 1998, **80**, 3803–3806.
4 S. Godefroo, M. Hayne, M. Jivanescu, A. Stesmans, M. Zacharias, O. I. Lebedev, G. Van Tendeloo and V. V. Moshchalkov, *Nat. Nanotechnol.*, 2008, **3**, 174–178.
5 M. Vörös, T. Demjén, T. Szilvási and A. Gali, *Phys. Rev. Lett.*, 2012, **108**, 267401.
6 T. Rander, M. Staiger, R. Richter, T. Zimmermann, L. Landt, D. Wolter, J. E. Dahl, R. M. K. Carlson, B. A. Tkachenko, N. A. Fokina, P. R. Schreiner, T. Möller and C. Bostedt, *J. Chem. Phys.*, 2013, **138**, 024310.
7 T. Zimmermann, R. Richter, A. Knecht, A. A. Fokin, T. V. Koso, L. V. Chernish, P. A. Gunchenko, P. R. Schreiner, T. Möller and T. Rander, *J. Chem. Phys.*, 2013, **139**, 084310.
8 A. Patzer, M. Schütz, T. Möller and O. Dopfer, *Angew. Chem., Int. Ed.*, 2012, **51**, 4925–4929.
9 K. Lenzke, L. Landt, M. Hoener, H. Thomas, J. E. Dahl, S. G. Liu, R. M. K. Carlson, T. Möller and C. Bostedt, *J. Chem. Phys.*, 2007, **127**, 084320.

This journal is © the Owner Societies 2014

Phys. Chem. Chem. Phys., 2014, **16**, 3070–3076 | **3075**

10 R. Meinke, R. Richter, T. Möller, B. A. Tkachenko, P. R. Schreiner, C. Thomsen and J. Maultzsch, *J. Phys. B: At., Mol. Opt. Phys.*, 2013, **46**, 025101.

11 Y. Wang, E. Kioupakis, X. Lu, D. Wegner, R. Yamachika, J. E. Dahl, R. M. K. Carlson, S. G. Louie and M. F. Crommie, *Nat. Mater.*, 2008, **7**, 38–42.

12 T. Willey, C. Bostedt, T. van Buuren, J. E. Dahl, S. Liu, R. M. K. Carlson, R. Meulenberg, E. Nelson and L. Terminello, *Phys. Rev. B: Condens. Matter Mater. Phys.*, 2006, **74**, 205432.

13 A. A. Fokin, P. R. Schreiner, N. A. Fokina, B. A. Tkachenko, H. Hausmann, M. Serafin, J. E. P. Dahl, S. Liu and R. M. K. Carlson, *J. Org. Chem.*, 2006, **71**, 8532–8540.

14 N. Drummond, A. Williamson, R. Needs and G. Galli, *Phys. Rev. Lett.*, 2005, **95**, 096801.

15 H. Ishiwata, Y. Acremann, A. Scholl, E. Rotenberg, O. Hellwig, E. Dobisz, A. Doran, B. A. Tkachenko, A. A. Fokin, P. R. Schreiner, J. E. P. Dahl, R. M. K. Carlson, N. Melosh, Z.-X. Shen and H. Ohldag, *Appl. Phys. Lett.*, 2012, **101**, 163101.

16 F. Marsusi, J. Sabbaghzadeh and N. D. Drummond, *Phys. Rev. B: Condens. Matter Mater. Phys.*, 2011, **84**, 245315.

17 W. A. Clay, T. Sasagawa, A. Iwasa, Z. Liu, J. E. Dahl, R. M. K. Carlson, M. Kelly, N. Melosh and Z.-X. Shen, *J. Appl. Phys.*, 2011, **110**, 093512.

18 H. Schwertfeger, A. A. Fokin and P. R. Schreiner, *Angew. Chem., Int. Ed.*, 2008, **47**, 1022–1036.

19 B. J. Waclawski, *J. Vac. Sci. Technol.*, 1982, **21**, 368.

20 A. T. Balaban and P. V. Ragué Schleyer, *Tetrahedron*, 1978, **34**, 3599–3609.

21 T. M. Willey, C. Bostedt, T. van Buuren, J. E. Dahl, S. G. Liu, R. M. K. Carlson, L. J. Terminello and T. Möller, *Phys. Rev. Lett.*, 2005, **95**, 113401.

22 J. E. Dahl, S. G. Liu and R. M. K. Carlson, *Science*, 2003, **299**, 96–99.

23 C. E. Patrick and F. Giustino, *Nat. Commun.*, 2013, **4**, 2006.

24 H. Schwertfeger, M. Machuy, C. Würtele, J. E. Dahl, R. M. Carlson and P. Schreiner, *Adv. Synth. Catal.*, 2010, **352**, 609–615.

25 A. A. Fokin, L. V. Chernish, P. A. Gunchenko, E. Y. Tikhonchuk, H. Hausmann, M. Serafin, J. E. P. Dahl, R. M. K. Carlson and P. R. Schreiner, *J. Am. Chem. Soc.*, 2012, **134**, 13641–13650.

26 J. E. P. Dahl, J. M. Moldowan, Z. Wei, P. A. Lipton, P. Denisevich, R. Gat, S. Liu, P. R. Schreiner and R. M. K. Carlson, *Angew. Chem., Int. Ed.*, 2010, 1–6.

27 H. Schwertfeger, C. Würtele, H. Hausmann, J. E. Dahl, R. M. Carlson, A. Fokin and P. Schreiner, *Adv. Synth. Catal.*, 2009, **351**, 1041–1054.

28 G. Fischer, *Int. Rev. Phys. Chem.*, 1986, **5**, 127–132.

29 G. Reichardt, J. Bahrdt, J.-S. Schmidt, W. Gudat, A. Ehresmann, R. Müller-Albrecht, H. Molter, H. Schmoranzer, M. Martins, N. Schwentner and S. Sasaki, *Nucl. Instrum. Methods Phys. Res., Sect. A*, 2001, **467–468**, 462–465.

30 A. Grinvald and I. Z. Steinberg, *Anal. Biochem.*, 1974, **59**, 583–598.

31 D. Wolter, PhD thesis, Technische Universität Berlin, 2012.

32 L. Landt, PhD thesis, Technische Universität Berlin, 2010.

33 J. Franck and E. G. Dymond, *Trans. Faraday Soc.*, 1926, **21**, 536.

34 E. Condon, *Phys. Rev.*, 1928, **32**, 858–872.

35 F. Santoro, R. Improta, A. Lami, J. Bloino and V. Barone, *J. Chem. Phys.*, 2007, **126**, 084509.

36 V. Barone, J. Bloino, M. Biczysko and F. Santoro, *J. Chem. Theory Comput.*, 2009, **5**, 540–554.

37 M. J. Frisch, G. W. Trucks, H. B. Schlegel, G. E. Scuseria, M. A. Robb, J. R. Cheeseman, G. Scalmani, V. Barone, B. Mennucci, G. A. Petersson, H. Nakatsuji, M. Caricato, X. Li, H. P. Hratchian, A. F. Izmaylov, J. Bloino, G. Zheng, J. L. Sonnenberg, M. Hada, M. Ehara, K. Toyota, R. Fukuda, J. Hasegawa, M. Ishida, T. Nakajima, Y. Honda, O. Kitao, H. Nakai, T. Vreven, J. A. Montgomery, J. E. Peralta, F. Ogliaro, M. Bearpark, J. J. Heyd, E. Brothers, K. N. Kudin, V. N. Staroverov, R. Kobayashi, J. Normand, K. Raghavachari, A. Rendell, J. C. Burant, S. S. Iyengar, J. Tomasi, M. Cossi, N. Rega, J. M. Millam, M. Klene, J. E. Knox, J. B. Cross, V. Bakken, C. Adamo, J. Jaramillo, R. Gomperts, R. E. Stratmann, O. Yazyev, A. J. Austin, R. Cammi, C. Pomelli, J. W. Ochterski, R. L. Martin, K. Morokuma, V. G. Zakrzewski, G. A. Voth, P. Salvador, J. J. Dannenberg, S. Dapprich, A. D. Daniels, Ö. Farkas, J. B. Foresman, J. V. Ortiz, J. Cioslowski and D. J. Fox, *Gaussian 09 Revision A.02*, Gaussian Inc., Wallingford, CT, 2009.

38 F. Duschinsky, *Acta Physicochim. URSS*, 1937, **7**, 551–566.

39 P. T. Ruhoff, *Chem. Phys.*, 1994, **186**, 355–374.

40 T. Yanai, D. P. Tew and N. C. Handy, *Chem. Phys. Lett.*, 2004, **393**, 51–57.

41 R. Krishnan, J. S. Binkley, R. Seeger and J. A. Pople, *J. Chem. Phys.*, 1980, **72**, 650.

42 J. O. Jensen, *Spectrochim. Acta, Part A*, 2004, **60**, 1895–1905.

43 M. Vörös and A. Gali, *Phys. Rev. B: Condens. Matter Mater. Phys.*, 2009, **80**, 161411.

44 J. W. Raymonda, *J. Chem. Phys.*, 1972, **56**, 3912.

45 M. Petitjean, *J. Math. Phys.*, 1999, **40**, 4587.

46 J. Petersen and R. Mitrić, personal communication.